20th International Conference on Composite Structures
Paris, 4-7th September 2017

Electro-Thermo-Structural Coupling Analysis on Lightning Damage of CFRP Laminates

Qi Dong, Yunli Guo, Yuxi Jia*

School of Materials Science and Engineering
Shandong University, Jinan 250061, China
dongqi_sdu@foxmail.com ; jia_yuxi@sdu.edu.cn

Contents

1.1 CFRP Composites

Bear the force

Bond and protect fibers

Reinforcement Carbon Fiber + **Matrix** resin = **Composite** CFRP

Interface

Transfer load

Good electrical conductivity

Dielectric

Semi-conductor

Laminated structure

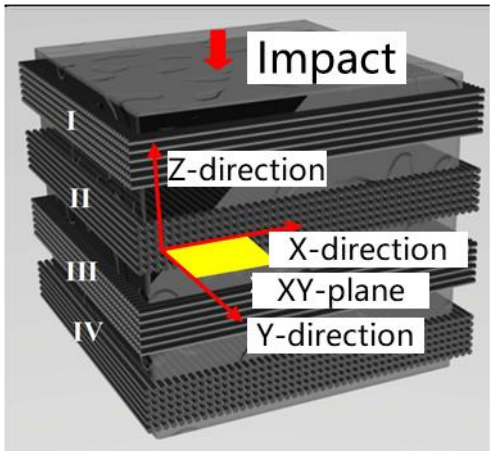

（Obtained from AVIC Composite Corporation LTD）

The advantages:

- **High strength**
- **High modulus**
- **Lightweight**
- **Good corrosion resistance**
- **Outstanding design ability**

For CFRP laminated structure, the excellent mechanical properties of in-plane directions can be obtained by lay-up design, but the existence of interlayer brittleness makes the composite structure sensitive to transverse impact.

1.2 CFRP in Boeing 787

- Carbon laminate
- Carbon sandwich
- Other composites
- Aluminum
- Titanium

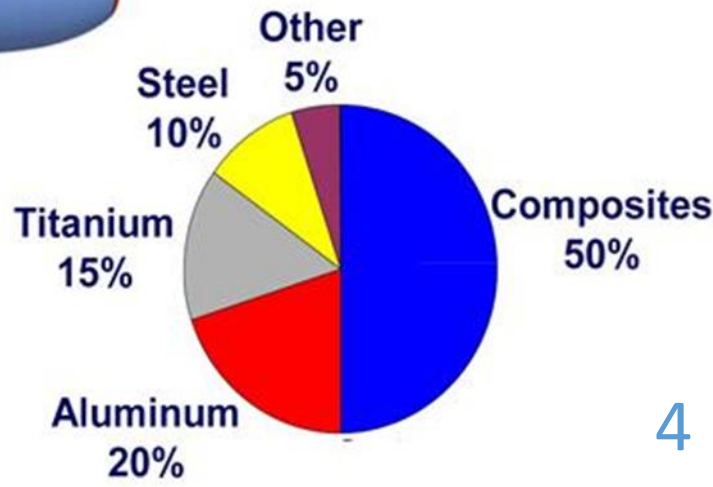

1.3 Interaction between lightning and aircraft

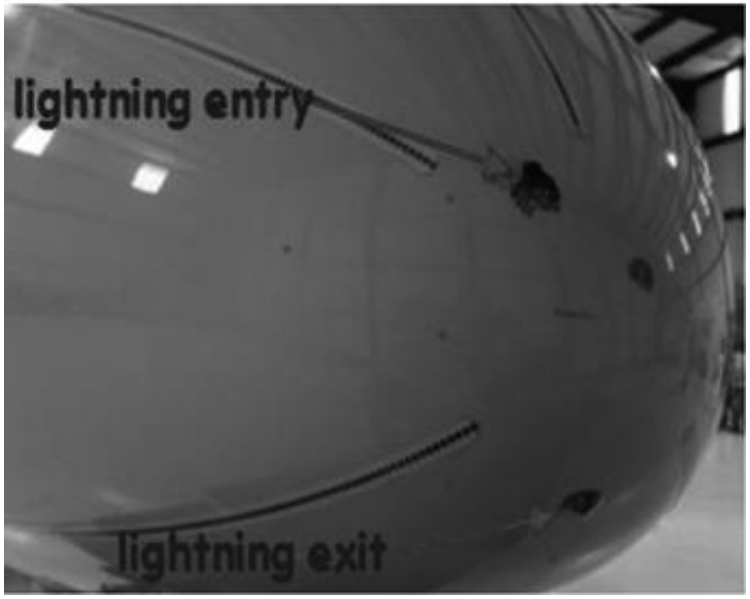

According to statistics, commercial aircraft will be struck **every 3,000 flight hours**, or about **once a year**.

Lightning strike poses a serious threat to all aircraft, as **the temperature will be 30,000℃** and **the pressure will exceed 10 atmospheres** in a lightning ionized leader channel.

Compared with metals, the relatively poor electrical conductivity of CFRP laminates makes carbon fiber based aircraft quite vulnerable to lightning strikes.

1.4 Lightning direct effects

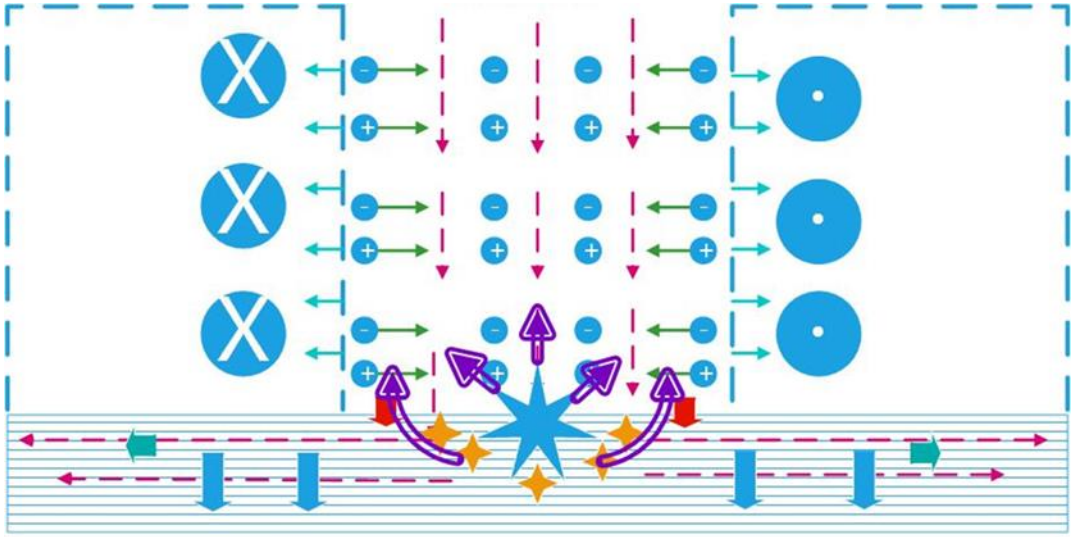

Fig. 1.1 Schematic diagram of lightning interaction with CFRP laminate

CFRP will suffer serious thermal ablation damage including fiber breakage, resin degradation, and delamination induced by lightning direct effects such as lightning arc heating, resistive heating, blow-off of pyrolytic gas, electro-magnetic forces and over-pressure shockwave.

Contents

2.1 Thermal transfer governing equation

Fourier's heat conduction equation [1]

$$c(T)\rho(T)\frac{\partial T}{\partial t}=k_{xx}(T)\frac{\partial^2 T}{\partial x^2}+k_{yy}(T)\frac{\partial^2 T}{\partial y^2}+k_{zz}(T)\frac{\partial^2 T}{\partial z^2}+q(t) \qquad \text{Eq. 1}$$

Thermal energy absorbed by material

$$q(t)=Q_S+Q_J+Q_P \qquad \text{Eq. 2}$$

Surface heat flux injection

$$Q_S=\frac{I(t)}{\pi R^2(t_r)}exp\left(\frac{r^2 ln(0.1)}{\left(0.55R(t_r)\right)^2}\right) \qquad \text{Eq. 3}$$

Joule heat

$$Q_J=J\cdot E=\sigma\cdot E\cdot E \qquad \text{Eq. 4}$$

Pyrolytic heat

$$Q_P=-\rho(T)H\frac{\partial \alpha}{\partial t} \qquad \text{Eq. 5}$$

[1] Abdelal G, Murphy A. Nonlinear numerical modelling of lightning strike effect on composite panels with temperature dependent material properties. Composite Structures 2014;109:268-278.

2.2 Pyrolysis kinetics equation

The CFRP decomposition behaviors can be described by the pyrolysis kinetic equations as follows [2].

Pyrolysis degree, *α*

$$\alpha = \frac{m_i - m}{m_i - m_f} \quad \text{Eq.6}$$

Kinetics equation, d*α*/d*t*

$$\frac{d\alpha}{dt} = k(T)(1-\alpha)^n \quad \text{Eq.7}$$

Rate constant, *k*(T) in Arrhenius expression

$$k(T) = A\exp\left(\frac{-E}{RT}\right) \quad \text{Eq.8}$$

***α* expression in difference method**

$$\alpha_i = \alpha_{i-1} + A\exp\left(\frac{-E}{RT_i}\right)(1-\alpha_{i-1})^n (t_i - t_{i-1}) \quad \text{Eq.9}$$

[2] Dong Q, Guo Y, Sun X, Jia Y. Coupled electrical-thermal-pyrolytic analysis of carbon fiber/epoxy composites subjected to lightning strike. Polymer 2015;56:385-394.

2.3 Damage constitutive formulation

- When the three dimensional mechanical damage tensor *D* is introduced to the stress-strain relationship, **the damage constitutive formulation** can be defined as:

$$\{\sigma\} = \boldsymbol{C}^{d,\,m}\{\varepsilon\} \qquad \text{Eq. 10}$$

$$\boldsymbol{C}^{d,\,m} = \left[C_{ij}^{d,\,m}\right]$$

$$= \begin{bmatrix} (1\text{-}d_1)C_{11} & (1\text{-}d_1)(1\text{-}d_2)C_{12} & (1\text{-}d_1)(1\text{-}d_3)C_{13} & & & \\ & (1\text{-}d_2)C_{22} & (1\text{-}d_2)(1\text{-}d_3)C_{23} & & & \\ & & (1\text{-}d_3)C_{33} & & & \\ & & & (1\text{-}d_1)(1\text{-}d_2)C_{44} & & \\ & sym. & & & (1\text{-}d_1)(1\text{-}d_3)C_{55} & \\ & & & & & (1\text{-}d_2)(1\text{-}d_3)C_{66} \end{bmatrix}$$

- The **stiffness matrix affected by thermal-mechanical coupling damage** can be expressed as:

$$\boldsymbol{C}^{d} = \begin{cases} \boldsymbol{C}^{d,\,m} & \alpha = 0 \\ (1\text{-}\alpha)\boldsymbol{C}^{d,\,m} & 0 < \alpha < 0.99 \\ 0.0001\boldsymbol{C}^{d,\,m} & \alpha \geq 0.99 \end{cases} \qquad \text{Eq. 11}$$

2.3 Damage constitutive formulation

Continuum damage mechanics

- Strain-based **Hashin failure criteria** are selected to judge the in-plane mechanical failure modes of fiber and matrix failures in tension and compression. **Yeh delamination failure criteria** are selected to **judge** the out-plane **mechanical failure mode** [3].

Fiber tensile mode ($\varepsilon_{11}>0$)

$$F_1^2=\left(\frac{\varepsilon_{11}}{\varepsilon_{1t}^f}\right)^2+\left(\frac{\gamma_{12}}{\gamma_{12}^f}\right)^2+\left(\frac{\gamma_{13}}{\gamma_{13}^f}\right)^2 \quad \textbf{Eq. 12}$$

Fiber compressive mode ($\varepsilon_{11}<0$)

$$F_1^2=\left(\frac{\varepsilon_{11}}{\varepsilon_{1c}^f}\right)^2 \quad \textbf{Eq. 13}$$

Matrix tensile mode ($\varepsilon_{22}+\varepsilon_{33}>0$)

$$F_2^2=\left(\frac{\varepsilon_{22}+\varepsilon_{33}}{\varepsilon_{2t}^f}\right)^2+\frac{\gamma_{23}^2-\varepsilon_{22}\varepsilon_{33}}{(\gamma_{23}^f)^2}+\left(\frac{\gamma_{12}}{\gamma_{12}^f}\right)^2+\left(\frac{\gamma_{13}}{\gamma_{13}^f}\right)^2 \quad \textbf{Eq. 14}$$

Matrix compressive mode ($\varepsilon_{22}+\varepsilon_{33}<0$)

$$F_2^2=\left[\left(\frac{\varepsilon_{2c}^f}{2\gamma_{23}^f}\right)^2-1\right]\frac{\varepsilon_{22}+\varepsilon_{33}}{\varepsilon_{2c}^f}+\left(\frac{\varepsilon_{22}+\varepsilon_{33}}{2\gamma_{23}^f}\right)^2-\frac{\varepsilon_{22}\varepsilon_{33}}{(\gamma_{23}^f)^2}+\left(\frac{\gamma_{12}}{\gamma_{12}^f}\right)^2+\left(\frac{\gamma_{13}}{\gamma_{13}^f}\right)^2+\left(\frac{\gamma_{23}}{\gamma_{23}^f}\right)^2$$

Eq. 15

Tensile delamination mode ($\varepsilon_{33}>0$)

$$F_3^2=\left(\frac{\varepsilon_{33}}{\varepsilon_{3t}^f}\right)^2+\left(\frac{\gamma_{13}}{\gamma_{13}^f}\right)^2+\left(\frac{\gamma_{23}}{\gamma_{23}^f}\right)^2 \quad \textbf{Eq. 16}$$

Shear delamination mode ($\varepsilon_{33}<0$)

$$F_3^2=\left(\frac{\gamma_{13}}{\gamma_{13}^f}\right)^2+\left(\frac{\gamma_{23}}{\gamma_{23}^f}\right)^2 \quad \textbf{Eq. 17}$$

[3] Huang CH, Lee YJ. Experiments and simulation of the static contact crush of composite laminated plates. Composite Structures 2003;61(3):265-270.

2.3 Damage constitutive formulation

- **Once the failure index *F* approaches the value of one at a point in the material, the properties of that point should be degraded to reflect the damage of material.**

  There are various methods to **define the relation between damage variable and failure index,** among which **the exponential damage evolution law** has been proved to be effective and with good convergence. When the initial failure criterion is satisfied, the damage variables can be defined as follows:

$$d_i = 1 - \frac{1}{F_i} e^{C_{ii}\left(\varepsilon_i^f\right)^2 L_C(1-F_i)/G_i^c} \quad (i=1, 2, 3) \qquad \text{Eq. 18}$$

where L_C is the characteristic length of the finite elements, G^c_i (i=1, 2, 3) is the fracture energy in longitudinal, in-plane transverse, and out-plane transverse directions, respectively.

Contents

3.1 Finite element model

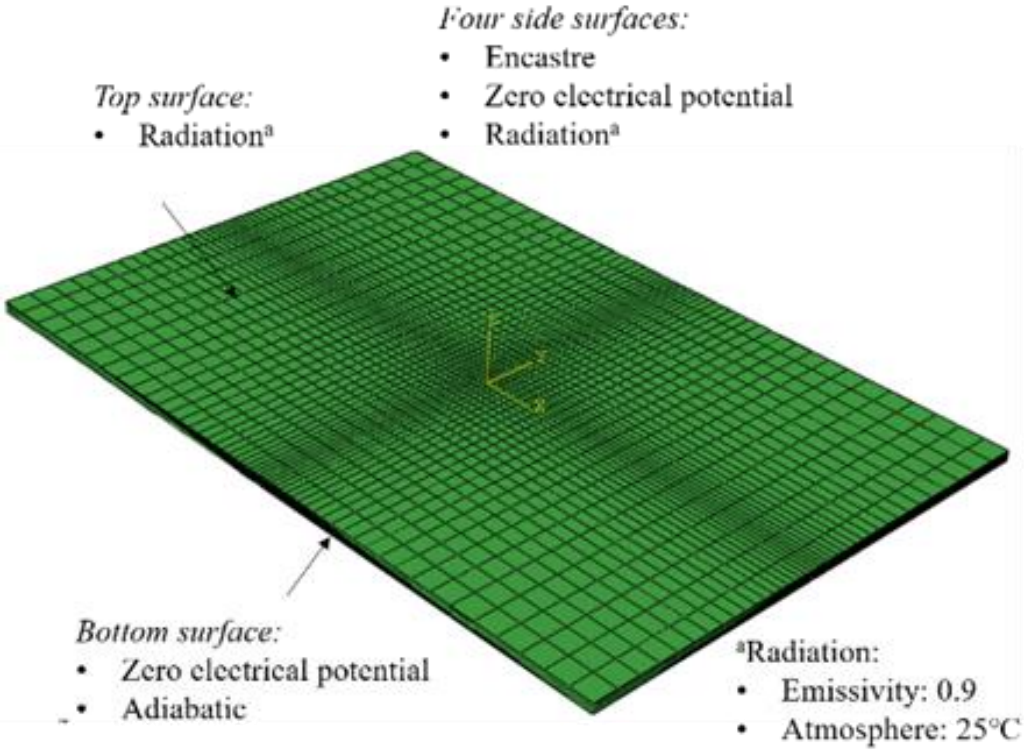

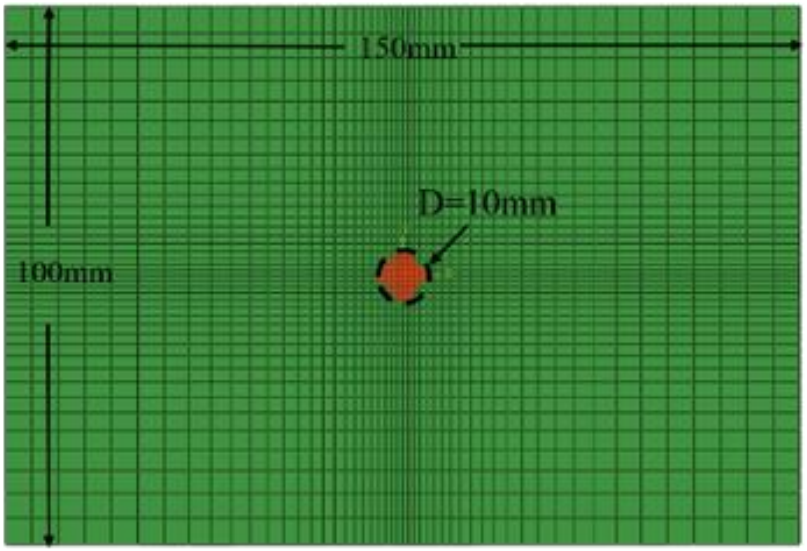

Notes:
- The red regions refer to the lightning attachment region.
- The black dotted lines refer to the ~10mm diameter lightning arc channel.

Fig. 3. 1 FEM model and boundary conditions

- **The laminate panel had three dimensions of 150×100×2 mm^3 containing 16 layers with a stacking sequence of $[45/0/-45/90]_{2s}$, and was meshed with 32000 elements.**
- **All displacements and rotations of the four side surfaces were constrained.**

3.2 Electrical boundary

1. The lightning arc was considered as a vertically downward cylinder with the diameter of 10 mm and applied at the center region of top surface, satisfying Gaussian distribution and being a function of time according to the test.

Current density $$J(r,t)=\frac{I(t)}{\pi R^2(t_r)}exp\left(\frac{r^2 ln(0.1)}{\left(0.55R(t_r)\right)^2}\right)$$ **Eq. 19**

2.1 The voltage of the bottom surface was presumed to be zero because it was contacted with grounding copper.

2.2 The voltage of the four side surfaces was presumed to be zero because the lightning discharge to the grounding copper was observed .

3.3 Thermal boundary

3. The surface heat flux, satisfying Gaussian distribution and being a function of time according to the lightning current waveform, was defined in ABAQUS subroutine DFLUX and applied within the lightning channel.

Surface heat flux

$$Q_S = \frac{I(t)}{\pi R^2(t_r)} exp\left(\frac{r^2 ln(0.1)}{\left(0.55R(t_r)\right)^2}\right)$$

Eq. 3

4. Thermal radiation was defined for the top surface except for lightning attachment area, whereas the bottom surface was assumed adiabatic.

3.4 Finite element simulation

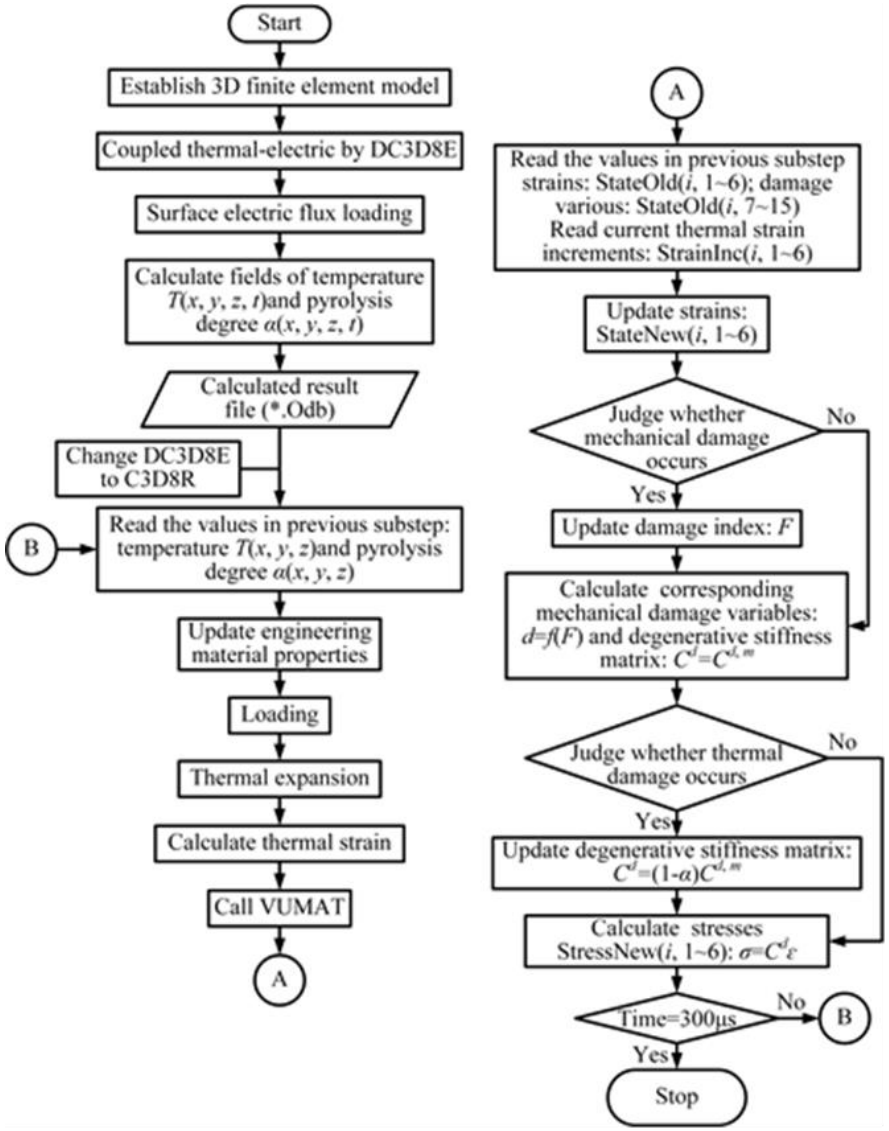

Fig. 3. 2 Flow chart of numerical simulation

Contents

4.1 Experimental conditions

To verify the feasibility of numerical method, the experimental verification of the material system of **TR50S15L/YPH-308** was conducted.

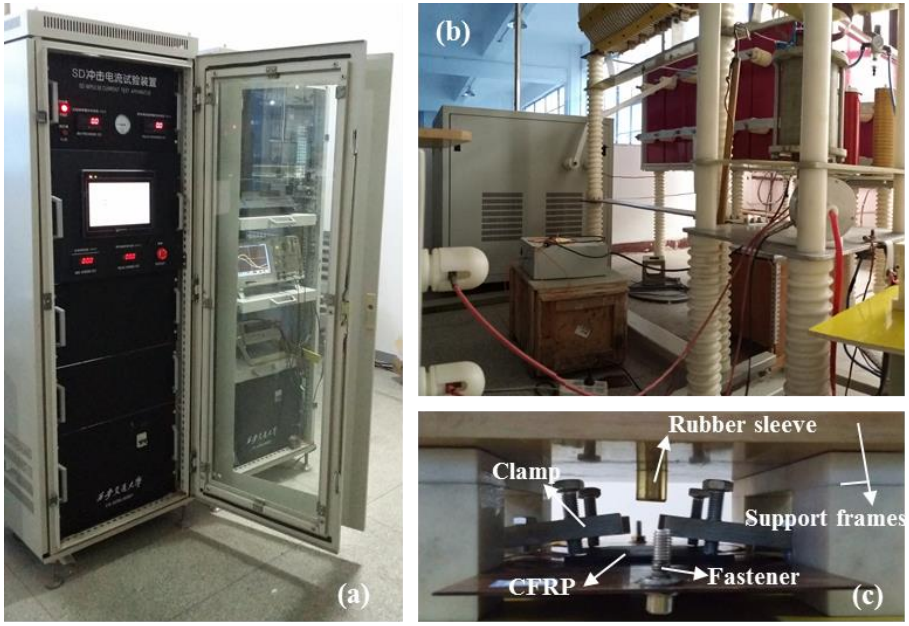

Fig. 4.1 Images of lightning strike test equipment.
(a) Control cabinet, (b) impulse current generator, (c) test setup.

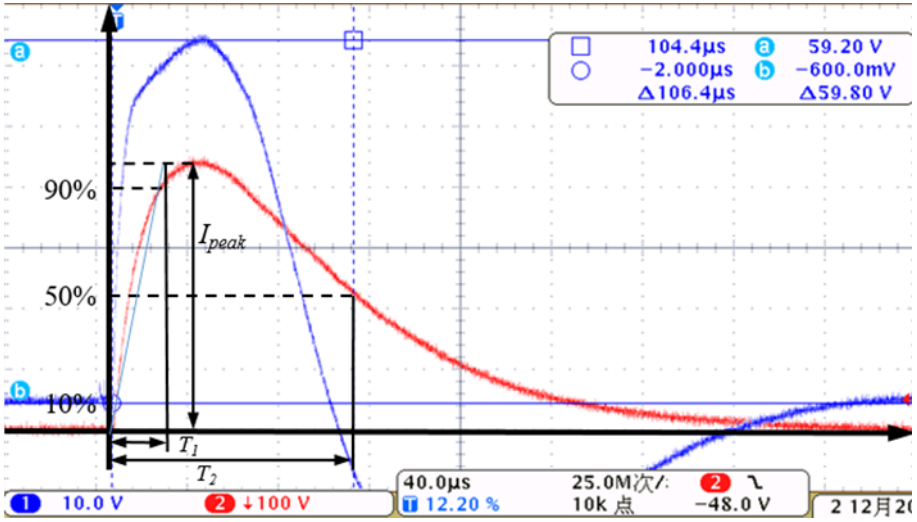

Fig. 4.2 Lightning current waveform (T_1/T_2=36.4/106.4 μs, I_{peak}=43.6 kA) in artificial lightning strike tests

4.2 Temperature field

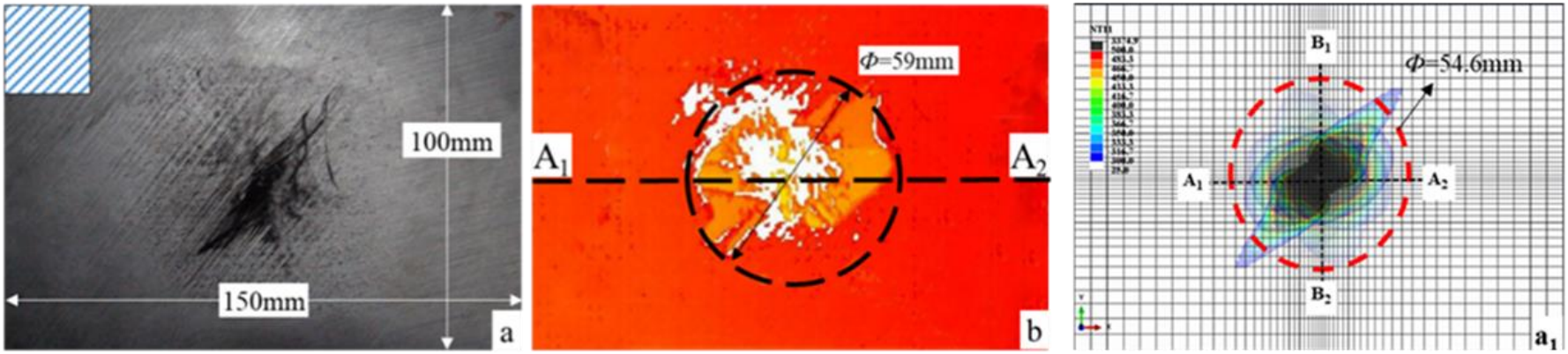

Fig. 4.3 Damage comparisons between the experiment and simulated temperature fields of TR50S15L/YPH-308 under 4/20 μs, 40 kA: (a) digital photograph, (b) ultrasonic C-scan, (a_1) overlap of isotherms ranging from 300 ºC~500 ºC

4.3 Pyrolysis degree field

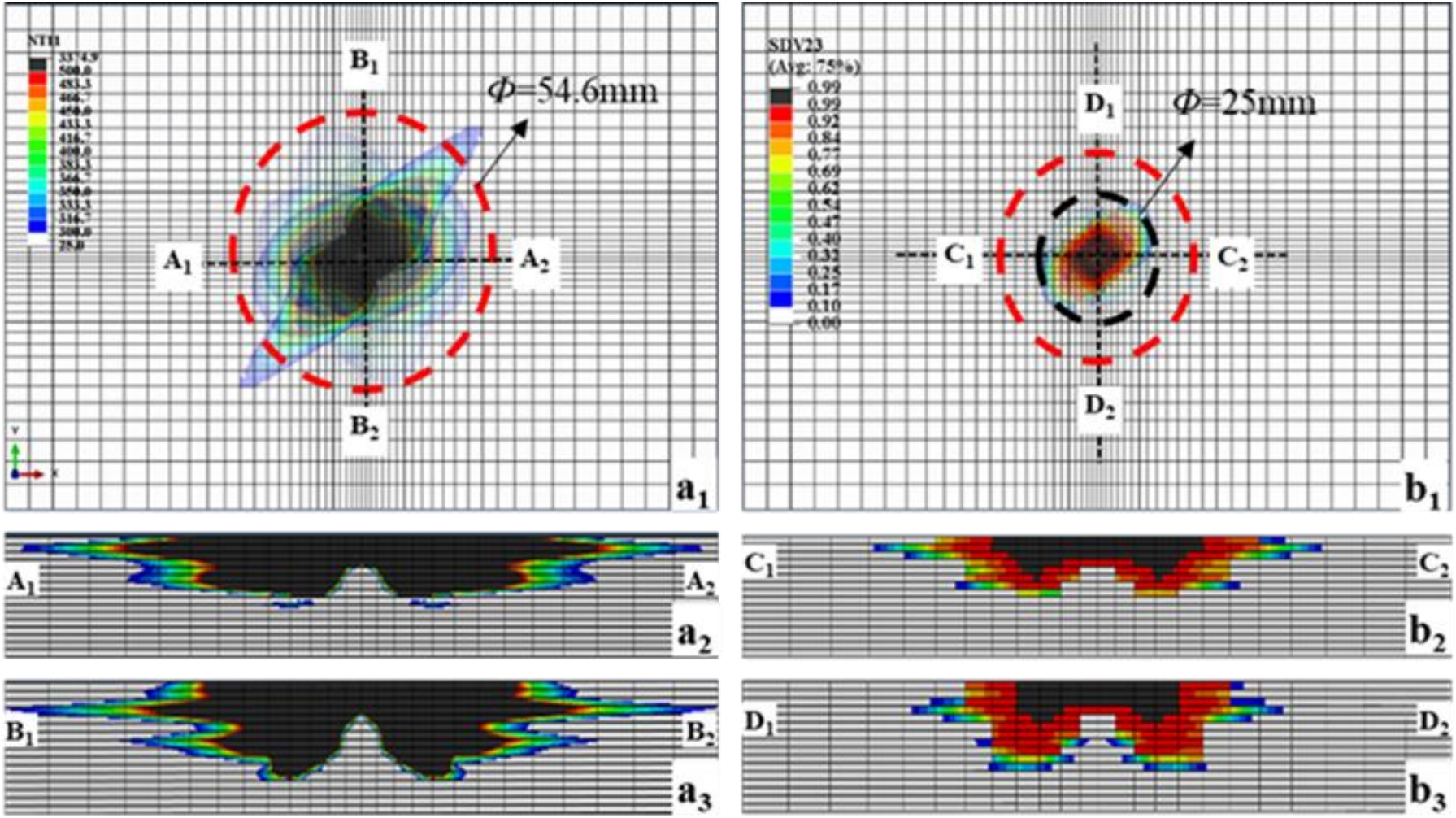

Fig. 4.4 Calculated fields of temperature and pyrolysis degree under the lightning waveform of 35/100 μs, 40 kA

4.4 Mechanical response under thermal expansion

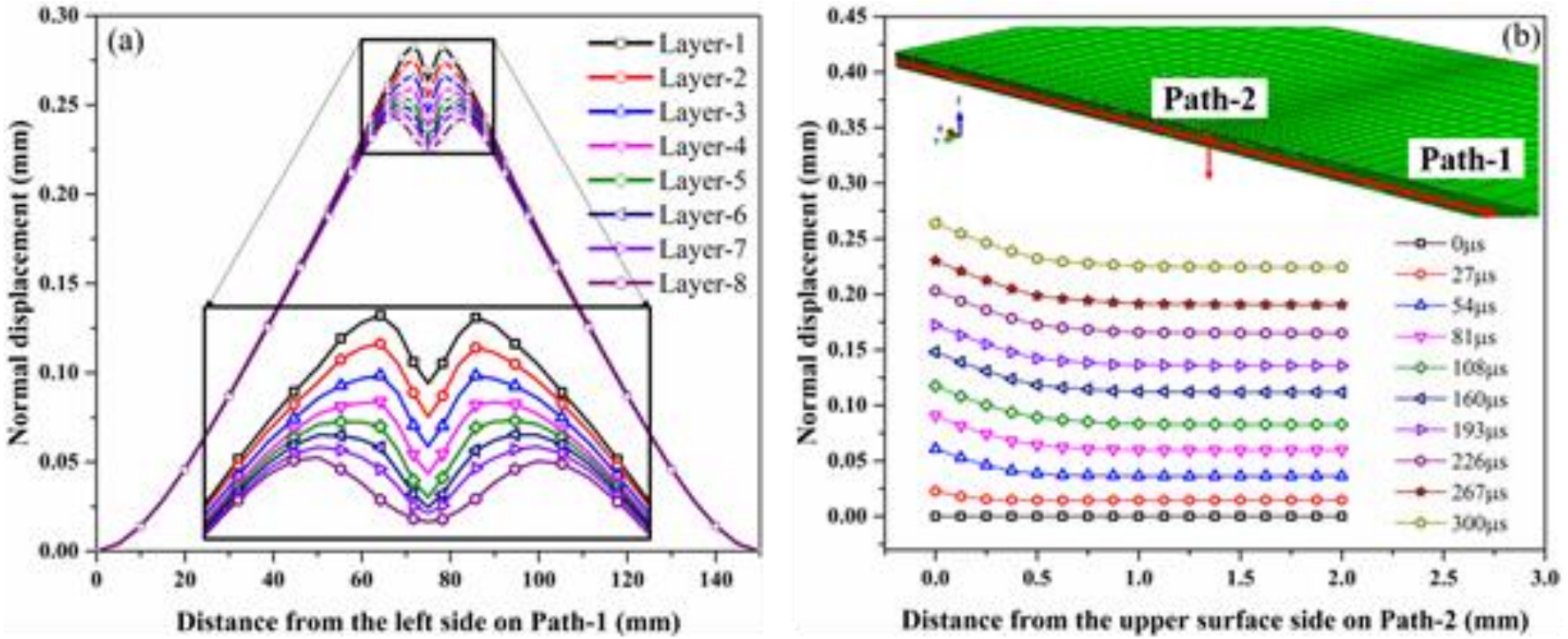

Fig. 4.5 Normal displacement curves along the defined paths on CFRP: (a) Path-1 of each layer at 300 μs, (b) Path-2 at different times

4.4 Mechanical response under thermal expansion

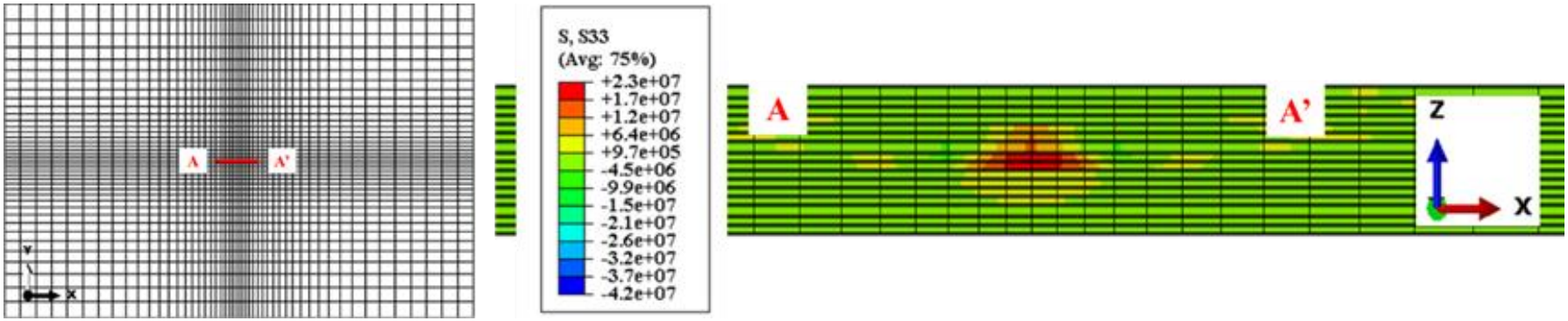

Fig. 4.6 Middle cross section view of stress component S33 at 300 μs

4.5 Delamination induced by thermal stress

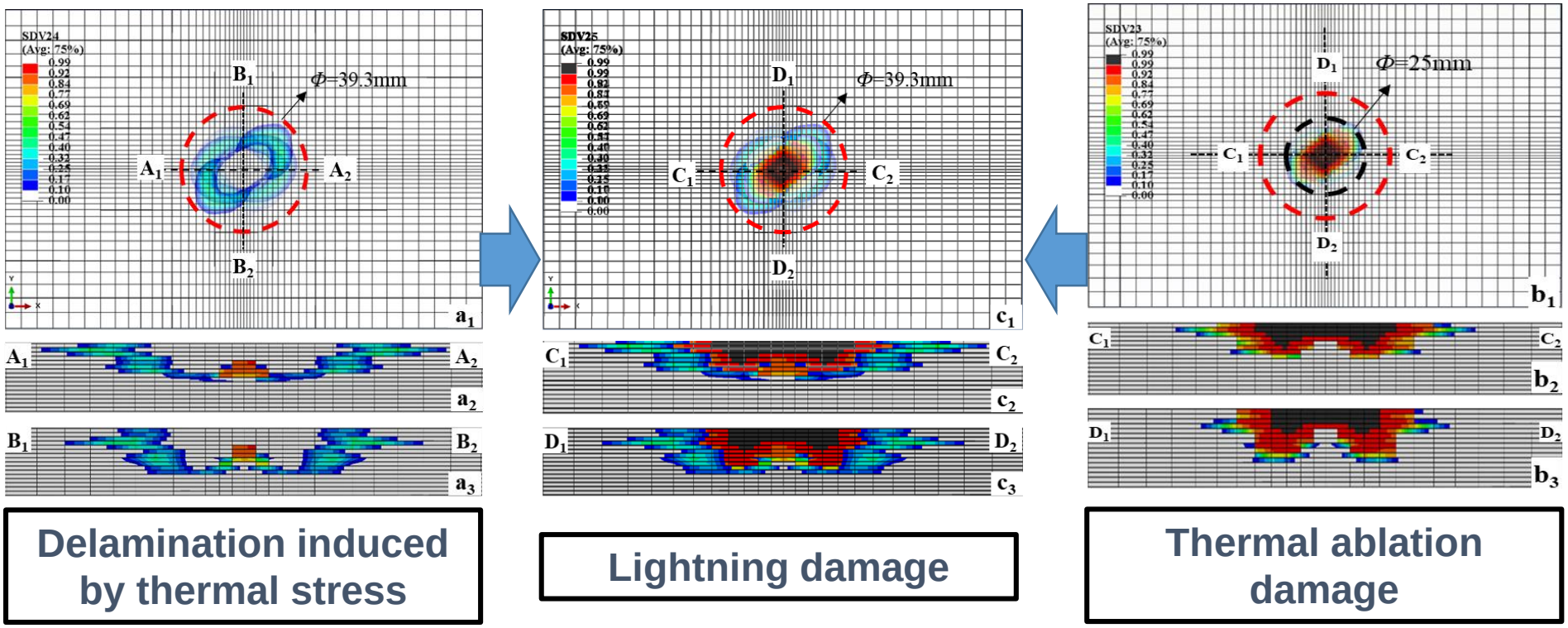

Fig. 4.7 Simulated damages under the lightning waveform of 35/100 μs, 40 kA: ($a_{1\sim3}$) delamination induced by thermal stress, ($b_{1\sim3}$) thermal ablation damage, ($c_{1\sim3}$) lightning damage

4.6 Verification

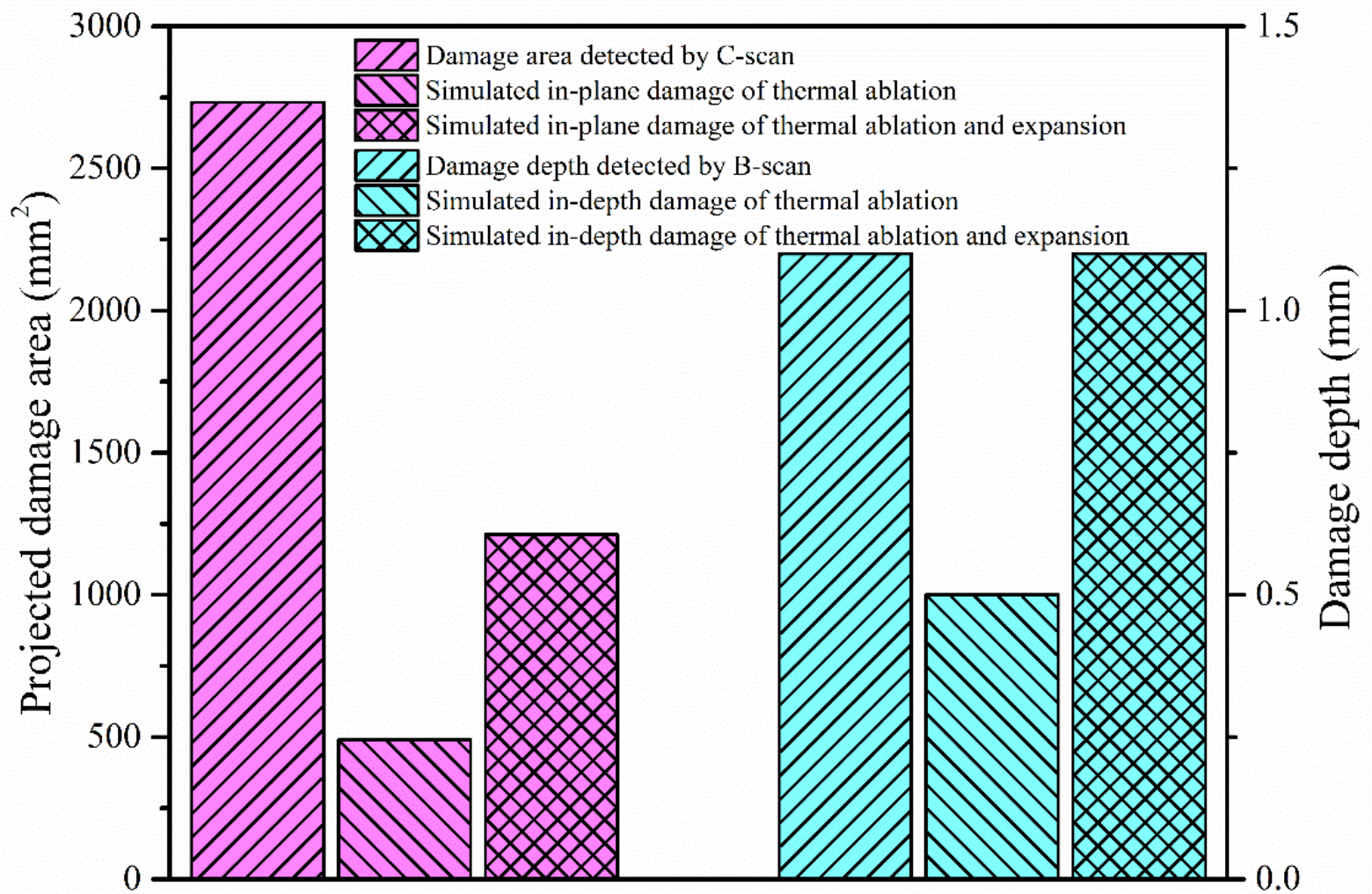

Fig. 4.8 Quantitative comparison of lightning damage between the experiment and simulations under the lightning waveform of 35/100 μs, 40 kA.

Contents

5 Conclusions

(1) The **degradation model of stiffness matrix** affected by lightning induced **thermal-mechanical coupling damage** is established to characterize the damage behavior of CFRP under thermal expansion effect, and then the damages are evaluated by comparison with the experiment.

(2) The **thermal stress** contributes to **a notable in-plane damage**, which is about 1.5 times than that of the thermal ablation damage, but there still exits a large deviation of in-plane damage between the experiment and simulation, which indicates the **explosion of pyrolytic gas** might contribute **more than 50% of the in-plane damage**.

(3) When compared with the experiment, the thermal ablation and thermal stress contribute about 50% of the in-depth damage respectively, whereas the **explosion of pyrolytic gas** makes **little contribution** to the **in-depth damage**.

Thanks for your attention!

Qi Dong, Yunli Guo, Yuxi Jia*

School of Materials Science and Engineering
Shandong University, Jinan 250061, China
dongqi_sdu@foxmail.com ; jia_yuxi@sdu.edu.cn